Fast Full-Wave Solution that Eliminates the Low-Frequency Breakdown Problem in a Reduced System of Order One

Jianfang Zhu, *Student Member, IEEE*, and Dan Jiao, *Senior Member, IEEE*

***Abstract*— Full-wave solutions of Maxwell's equations break down at low frequencies. Existing methods for solving this problem either are inaccurate or incur additional computational cost. In this paper, a fast full-wave finite-element-based solution is developed to eliminate the low-frequency breakdown problem in a reduced system of order one. It is applicable to general 3-D problems involving ideal conductors as well as nonideal conductors immersed in inhomogeneous, lossless, lossy, and dispersive materials. The proposed method retains the rigor of a theoretically rigorous full-wave solution recently developed for solving the low-frequency breakdown problem, while eliminating the need for an eigenvalue solution. Instead of introducing additional computational cost to fix the low-frequency breakdown problem, the proposed method significantly speeds up the low-frequency computation.**

***Index Terms*— Electromagnetic analysis, fast solution, finite element methods, full-wave analysis, low-frequency breakdown, nullspace.**

I. Introduction

IT HAS been observed that a full-wave-based solution of Maxwell's equations breaks down at low frequencies. Such a problem is especially severe in digital and mixed-signal integrated circuit (IC) applications in which signals have a broad bandwidth from dc to about the third harmonic frequency. In these applications, full-wave solvers typically break down at and below tens of MHz, which are right in the range of circuit operating frequencies. Inaccurate low-frequency models can lead to erroneous and misleading results in the analysis and design of ICs and systems. The inaccuracy at low frequencies is also found to be the major contributor to the violation of passivity, stability, and causality in existing frequency-domain models, which leads to divergence in time-domain simulation. Therefore, there is a critical need to solve the low-frequency breakdown problem.

Existing solutions to the low-frequency breakdown problem can be categorized into two classes. One class is to stitch a static- or quasi-static-based electromagnetic solver with a full-wave-based electromagnetic solver. This approach is inaccurate because static/quasi-static solvers involve fundamental approximations such as decoupled **E** and **H**, which is only true at dc. Moreover, at which frequency to switch between different solvers is an issue. As often seen in practice, the stitched results may not reach a consensus at their interfaces. Engineers usually have to employ an approximation-based model to achieve a smooth transition between static, quasi-static, and full-wave solvers. Besides the issue of accuracy, such an artificially created model often violates passivity, stability, and causality. The other class of methods for solving the low-frequency breakdown problem is to extend the validity of full-wave solvers to low frequencies. Existing approaches that belong to this category include introducing the loop-tree and loop-star basis functions to achieve a natural Helmholtz decomposition of the current in integral-equation-based methods [2]; using the tree-cotree splitting to provide an approximate Helmholtz decomposition for edge elements in finite-element-based methods (FEM) [3], [4]; formulating current-charge integral equations and the augmented electric field integral equation [5], [6], and developing Calderon preconditioner-based methods [7], [8]. These methods have been successful in extending the capability of existing full-wave solvers to low frequencies that cannot be solved previously. They have also suggested a number of new research questions to be considered. For example, if a method does not provide a universal solution of Maxwell's equations from high frequencies down to any low frequency, then at which frequency should one switch to a different solution method? If a method utilizes certain low-frequency approximations, when are these approximations valid? And to what degree of accuracy? When a full-wave solution breaks down, is it true that natural or approximate Helmholtz decomposition can be used to produce accurate results? In other words, does a range of frequencies exist, in which neither traditional full-wave solvers (due to breakdown) nor natural or approximate Helmholtz decomposition (due to low-frequency approximations) can produce accurate results?

To address these questions, it becomes necessary to know the true solution of full-wave Maxwell's equations with **E** and **H** coupled from dc to high frequencies. Such a solution, which is a continuous function of frequency in a full electromagnetic spectrum, was derived in [1] and [9] without making use of theoretical approximations. In these two papers,

Manuscript received January 6, 2012; revised May 15, 2012; accepted May 16, 2012. Date of publication July 12, 2012; date of current version October 30, 2012. This work was supported in part by a grant from the Intel Corporation, a grant from the Office of Naval Research under Award N00014-10-1-0482, and a grant from NSF under Award 0747578. Recommended for publication by Associate Editor E.-P. Li upon evaluation of reviewers' comments.

The authors are with the School of Electrical and Computer Engineering, Purdue University, West Lafayette, IN 47907 USA (e-mail: zhu3@purdue.edu; djiao@purdue.edu).

Color versions of one or more of the figures in this paper are available online at http://ieeexplore.ieee.org.

Digital Object Identifier 10.1109/TCPMT.2012.2203135

it is shown that the root cause of low-frequency breakdown problem is finite machine precision. To bypass the barrier of finite machine precision, the method proposed in [1] and [9] transforms the original frequency-dependent deterministic problem to a frequency independent generalized eigenvalue problem. With the inexact zero eigenvalues fixed to be zero, the method successfully bypassed the barrier of finite machine precision, and solved the low-frequency breakdown problem with a universal solution that is valid at both high and low frequencies. Moreover, the frequency dependence of the solution to Maxwell's equations is explicitly revealed from dc to high frequencies. One can use the resultant analytical model of frequency dependence to develop a theoretical understanding on how the field solution should scale with frequency in both low- and high-frequency regimes; at which frequency full-wave effects become important; at which frequency static assumptions yield good accuracy; etc.

The problem considered in [1] and [9] is a purely lossless problem containing ideal dielectrics and perfect conductors or a purely lossy problem consisting of good conductors only. The low-frequency breakdown problem in general cases, that involve both inhomogeneous lossless/lossy dielectrics and nonideal conductors, is significantly complicated by the frequency-dependent coupling between dielectrics and nonideal conductors. In addition, the matrix resulting from the analysis of the metal-dielectric composite is highly unbalanced, which further complicates the low-frequency breakdown problem. In [10] and [11], this problem was successfully solved and a theoretically rigorous solution to Maxwell's equations was derived for general problems with inhomogeneous lossless and/or lossy dielectrics and nonideal conductors from dc to high frequencies. In [14], it is further shown that the method developed in [1] and [9]–[11] for a finite-element-based analysis is equally applicable to solve the low-frequency breakdown in an electric field integral equation.

The methods developed in [1], [9]–[11], and [14] require an eigenvalue solution of a large-scale system of $O(N)$ with $\mathbf{N}$ being the problem size. Although with advanced techniques, the eigenvalue solutions can also be found in linear complexity [12], [13], the resultant computational cost of solving the low-frequency problem is still not desirable. Additional computational cost is also observed in other existing methods for solving the low-frequency breakdown problem.

In this paper, without compromising accuracy, we propose a fast solution to eliminate the low-frequency breakdown problem in a full-wave solver. Such a fast solution is, in fact, a direct outcome of the theoretical model developed in [1] and [9]–[11] that explicitly reveals the frequency dependence of the solution to Maxwell's equations from dc to high frequencies. Such a theoretical model suggests that one can use one solution vector obtained from the traditional full-wave solver to reduce the original system of $O(N)$ to be a system of $O(1)$, and then fix the low-frequency breakdown problem readily in the reduced $O(1)$ system. In this way, we equally bypass the barrier of finite machine precision, preserve the theoretical rigor of the solution developed in [1] and [9]–[11], while obtaining the field solution at low frequencies including dc without introducing any additional computational cost. Instead, we accelerate the low-frequency computation by obtaining the field solution in $O(1)$ complexity when simulating a frequency band of interest from high to low frequencies.

In what follows, we first state the low-frequency breakdown problem; then present the proposed fast low-frequency full-wave solution. We will start with the proposed solution for solving problems with ideal conductors; then proceed to the solution for solving problems with nonideal conductors. The dielectrics can be inhomogeneous, lossless, lossy, or dispersive.

II. Low-Frequency Break-Down Problem

Consider a general 3-D electromagnetic problem that involves both inhomogeneous dielectric materials and nonideal conductors. A full-wave FEM-based analysis of such a problem results in the following matrix equation in frequency domain:

$$A(\omega)x(\omega) = b(\omega) \tag{1}$$

where ω is angular frequency, and

$$A(\omega) = S - \omega^2\mathbf{T} + j\omega\mathbf{R} \tag{2}$$

in which stiffness matrix $\mathbf{S}$, mass matrix $\mathbf{T}$, and conductivity related mass matrix $\mathbf{R}$ are assembled from their elemental contributions as follows:

$$\begin{aligned}
\mathbf{S}_{ij}^e &= \iiint_{V^e} \mu_r^{-1}(\nabla \times \mathbf{N}_i) \cdot (\nabla \times \mathbf{N}_j) dV \\
\mathbf{T}_{ij}^e &= \iiint_{V^e} \frac{\varepsilon_r}{c^2} \mathbf{N}_i \cdot \mathbf{N}_j dV \\
\mathbf{R}_{ij}^e &= \iiint_{V^e} \mu_0 \sigma \mathbf{N}_i \cdot \mathbf{N}_j dV + \frac{1}{c} \iint_{S_o} (\hat{n} \times \mathbf{N}_i) \cdot (\hat{n} \times \mathbf{N}_j) dS \\
b_i^e &= -j\omega\mu_0 \iiint_{V^e} \mathbf{N}_i \cdot \mathbf{J} dV.
\end{aligned} \tag{3}$$

In (3), c is the speed of light in free space, σ is conductivity, ε_r is relative permittivity, $\mathbf{J}$ represents a current source, $\mathbf{N}$ is the normalized vector basis function used to expand $\mathbf{E}$ field, and superscript e denotes the contribution from an element.

The solution of (1) breaks down at low frequencies. In [1] and [9], the root cause is shown to be finite machine precision, and a detailed analysis of the root cause has been given. Here, we give a brief summary. When frequency is low enough that the contribution of frequency dependent terms in (2), either $\omega^2\mathbf{T}$ or $j\omega\mathbf{R}$, is lost due to finite machine precision, breakdown occurs. When this happens, the solution of (1) can be completely wrong because stiffness matrix $\mathbf{S}$ is not invertible. To be specific, the value of $\mathbf{S}_{ij}$ is $O(l)$ because $\nabla \times \mathbf{N}$ is proportional to $1/l$, and the value of $\mathbf{T}_{ij}$ is proportional to $10^{-17}l^3$, where l is the average edge length used in a 3-D discretization of an electromagnetic structure. In state-of-the-art very-large-scale integration (VLSI) circuits, l is at the level of 1 μm. Hence, the ratio of $\mathbf{T}$'s norm over $\mathbf{S}$'s norm is in the order of 10^{-29}, which is significantly smaller than that in a microwave or millimeter wave circuit. Since the norm of $\mathbf{T}$ is 10^{-29} smaller than the norm of $\mathbf{S}$ in a VLSI circuit, at low frequencies where $\omega^2\mathbf{T}$ is 16 orders

of magnitude smaller than $\mathbf{S}$, even one uses double-precision computing, the mass matrix $\mathbf{T}$ is essentially treated as zero by computers when performing the addition of $\omega^2\mathbf{T}$ and $\mathbf{S}$. The same analysis applies to the lossy system where $\mathbf{R}$ exists.

III. Proposed Fast Low-Frequency Full-Wave Solution for Problems With Ideal Conductors

A. Theoretical Basis of the Proposed Fast Solution

The theoretical model of the true solution to Maxwell's equations from dc to high frequencies developed in [1] and [9] has provided a theoretical basis for the proposed fast solution. Next, we will use the lossless case that only involves ideal dielectrics and perfect conductors as an example to introduce this theoretical model. In a lossless case, (2) becomes

$$A(\omega) = S - \omega^2\mathbf{T}. \tag{4}$$

From [1] and [9], the solution of (4) can be obtained by solving the following generalized eigenvalue problem that is frequency independent:

$$\mathbf{S}\upsilon = \lambda\mathbf{T}\upsilon \tag{5}$$

where λ is eigenvalue and υ is eigenvector. Denoting the diagonal matrix formed by all the eigenvalues by Λ, and the matrix formed by all the eigenvectors by V, the inverse of (4) can be written as

$$[\mathbf{A}(\omega)]^{-1} = V(\Lambda - \omega^2\mathbf{I})^{-1}V^T \tag{6}$$

where $\mathbf{I}$ is an identity matrix. We also point out in [1] that the eigenvalues of (5) can be divided into two groups: one group is associated with physical dc modes as well as nonphysical ones originated from the nullspace of $\mathbf{S}$, and the other is associated with the nonzero resonance frequencies of the 3-D structure. The first group has zero eigenvalues. However, numerically they cannot be computed as exact zeros due to finite machine precision. Thus, we need to correct the inexact zeros to be exact zeros. With that, (6) becomes

$$\begin{aligned}[\mathbf{A}(\omega)]^{-1} &= (V_0\ V_h)\begin{bmatrix} -\omega^2\mathbf{I} & 0 \\ 0 & \Lambda_h - \omega^2\mathbf{I}\end{bmatrix}^{-1}(V_0\ V_h)^T \\ &= -\frac{1}{\omega^2}V_0V_0^T + V_h[\Lambda_h - \omega^2\mathbf{I}]^{-1}V_h^T \end{aligned}\tag{7}$$

where V_0 denotes the eigenvectors corresponding to zero eigenvalues, V_h and Λ_h denote the eigenvectors and eigenvalues corresponding to nonzero eigenvalues, i.e., higher order modes. As can be seen from (7), the frequency dependence of the solution to the full-wave FEM system matrix is explicitly derived. Except for ω, all the other terms are frequency independent. With such a continuous function of frequency, one can rigorously obtain the field solution from high frequencies down to any low frequency including dc without suffering from low-frequency breakdown.

To obtain a solution shown in (7) that is free of low-frequency breakdown, apparently, one has to first solve a generalized eigenvalue problem shown in (5), the computation of which could be nontrivial. In fact, with its analytical model of the frequency dependence, (7) already suggests a fast yet rigorous low-frequency full-wave solution that avoids the eigenvalue solution, which can be seamlessly incorporated into existing full-wave solvers to fix the breakdown problem readily. The details are given below.

From (7), it can be seen clearly that given any frequency ω, the field solution is the superposition of a number of 3-D eigenmodes. For a dc eigenmode, i.e., an eigenvector corresponding to zero eigenvalue, its weight in the field solution is proportional to $(1/\omega^2)$; for a higher order eigenmode, its weight in the field solution is proportional to $1/(\lambda_i - \omega^2)$, where λ_i is the corresponding eigenvalue. At low frequencies where the weight of the higher order eigenmodes is significantly smaller than that of the dc eigenmodes, the contribution of the higher order eigenmodes in the field solution is negligible. As a result, (7) can be written as

$$[\mathbf{A}(\omega)]^{-1} \overset{\varepsilon}{=} \left[-\frac{1}{\omega^2}V_0V_0^T\right] \tag{8}$$

the accuracy of which, ε, can be controlled to any desired order by choosing an ω that is low.

From (8), it is clear that at low frequencies where the contribution from higher order eigenmodes is negligible, the space where the field solution resides is the union of the dc eigenmodes V_0. In other words, the field solution resides in the nullspace of stiffness matrix $\mathbf{S}$. In (8), all the nullspace vectors should be included because they are linearly independent with each other and each of them is indispensable in building a complete nullspace. Given a 3-D structure, even though the number of physical dc modes could be a few, the nullspace is mixed with both physical dc modes and nonphysical ones. A linear combination of these two still resides in the same nullspace. As a result, solely from nullspace vectors, one cannot distinguish physical dc modes from nonphysical ones. Moreover, one cannot discard a subset of nullspace vectors to reduce the size of nullspace since the remaining ones are not complete. Given an excitation vector, it can have a projection onto all of the nullspace vectors, and hence each of the nullspace vectors can have a contribution to the field solution. However, if one keeps all the nullspace vectors, the resultant computational cost is high because the nullspace of stiffness matrix $\mathbf{S}$ is large and, also, grows with matrix size $\mathbf{N}$ linearly. Therefore, how to handle the increased size of the nullspace becomes critical in developing a fast low-frequency solution. Our solution to this problem is to utilize the fact that all the nullspace vectors share the same zero eigenvalue in common although their eigenvectors are completely different. Based on this fact, we propose to use the right-handside vector (excitation vector) to shrink the dimension of the space where the field solution resides. To explain, in a deterministic solution, the right-hand side is always known. In other words, we solve (1) for a given right-hand side $b(\omega)$. With $b(\omega)$, effectively, all the nullspace vectors are grouped together and the contribution from all the nullspace vectors can be represented by a single vector w_0 as shown below

$$x(\omega) = -\frac{1}{\omega^2}V_0V_0^Tb(\omega) = w_0. \tag{9}$$

In other words, the field solution vectors obtained at different frequencies are linearly dependent on each other, and hence

representing the same solution space. A grouping like (9) would not be possible if the eigenvectors do not share the same eigenvalue in common, which is the case for higher order eigenvectors V_h. As can be seen from (7), even by right multiplying with a right-hand-side vector $b(\omega)$, the eigenvectors V_h cannot be grouped together and represented by a one-vector-based space. This is because the contribution from each V_h is different at different frequencies in the field solution owing to the difference in eigenvalues. By right multiplying with $b(\omega)$, although the contribution from all the higher order eigenvectors also becomes a single vector, this vector can be linearly independent with each other at different frequencies.

What is implied by (9) is significant: given a right-hand side, only one vector is adequate to span the low-frequency solution. Although the above analysis is developed based on a lossless system shown in (4), in which both dieletrics and conductors are lossless, the finding that the field solutions at low frequencies can be fully represented by a reduced space of $O(1)$ is equally applicable to problems with dispersive and lossy dielectrics since the field solution still resides in the same nullspace of stiffness matrix $\mathbf{S}$. To be specific, for problems with inhomogeneous lossless and/or lossy dielectrics, $\mathbf{T}$ in (4) and (5) becomes a complex-valued matrix because of complex permittivity. At low frequencies where the contribution from higher order modes can be neglected, based on the analysis given in [11], (9) becomes

$$x(\omega) = -\frac{1}{\omega^2} V_0 (V^T \mathbf{T} V)^{-1} (V_0\ , V_h)^T b(\omega).$$

Since $(V^T \mathbf{T} V)^{-1}$ and V_h do not depend on frequency, again the above can be represented by a single-vector-based space at different frequencies. For problems filled by a dispersive material, $\mathbf{T}$ in (4) and (5) becomes frequency dependent because of frequency dependent permittivity. In this case, the $V_0 V_0^T$ in (9) will be scaled by a frequency dependent coefficient associated with relative permittivity, while the space represented by (9) is still of dimension 1 at different frequencies.

B. Proposed Fast Low-Frequency Full-Wave FEM Solution

Equation (9) serves as a theoretical basis for the proposed fast low-frequency full-wave solution of $O(1)$. As long as we can find the single vector w_0 that forms the $O(1)$ space in which all the low-frequency solutions reside, given a frequency regardless of how low it is, we can expand the field solution in this $O(1)$ space, and transform the original system of $O(N)$ shown in (1) to an $O(1)$ system, from which the low-frequency breakdown problem can be readily fixed.

To obtain w_0 and also avoid solving the generalized eigenvalue problem shown in (5), we developed the following approach. As can be seen from (8) and (9), at a low frequency where the contribution from higher order eigenmodes is negligible, the field solution $x(\omega)$ is in the space formed by a single vector w_0. Therefore, we can use one solution vector obtained at such a frequency as a complete and accurate representation of the space formed by w_0, i.e., the space where all the low-frequency solutions reside. Denoting such a frequency by f_{ref}, we solve the original system (1) as it is and obtain a single solution vector, which is denoted by x_{ref}. With x_{ref}, given any low frequency ω, we can expand the solution of the FEM-based system equation by using

$$x(\omega) = x_{\text{ref}} y \tag{10}$$

with unknown coefficient y solved as the following:

$$x_{\text{ref}}^T (S - \omega^2 \mathbf{T}) x_{\text{ref}} y = x_{\text{ref}}^T b(\omega). \tag{11}$$

As a result, the system is reduced to a one by one system. However, the low-frequency breakdown problem still remains in the reduced $O(1)$ system when the term associated with ω^2 is neglected due to finite machine precision. To fix this problem, as the theoretically rigorous solution developed in [1], we utilize the fact that $\mathbf{S} x_{\text{ref}} = 0$ to vanish $\mathbf{S} x_{\text{ref}}$. This can be done because, as can be seen from (9), x_{ref} is a nullspace vector that satisfies $\mathbf{S} V_0 = 0$. Therefore, (11) becomes

$$x_{\text{ref}}^T (-\omega^2 \mathbf{T}) x_{\text{ref}} y = x_{\text{ref}}^T b(\omega) \tag{12}$$

which can be solved at any low frequency without breakdown. With unknown coefficient y solved from (12), the field solution can be recovered from (10). In this way, we can rapidly fix the low-frequency breakdown problem, and meanwhile retaining the theoretical rigor of the low-frequency solution developed in [1] and [9].

The aforementioned solution is applicable to problems with inhomogeneous lossless and/or lossy dielectrics, as well as problems filled with a dispersive material. For the latter, at low frequencies, although the field solution still resides in the nullspace of $\mathbf{S}$, the solution could scale with frequency in a complicated way since $\mathbf{T}$ now becomes frequency dependent.

The remaining problem is whether we can always find an appropriate f_{ref}. This is discussed in the following section.

C. Existence of f_{ref} and Its Choice

The choice of f_{ref} is subject to two requirements. First, since we need to solve (1) at f_{ref} to obtain the field solution, the f_{ref} should be chosen at a frequency where the full-wave solution does not break down yet. Second, since we use the solution vector obtained at f_{ref} to represent the $O(1)$ space formed by w_0, the field solution at f_{ref} should have a form shown in (9). In other words, the field solution at f_{ref} should be dominated by dc eigenmodes, with the contribution from higher order eigenmodes negligible. To summarize, the f_{ref} should be a frequency at which the field solution is dominated by dc eigenmodes and meanwhile the full-wave solution does not break down yet. To choose f_{ref}, the first question we need to answer is whether such a frequency exists or not. To examine the existence of f_{ref}, we need to take a look at the relative relationship between the breakdown frequency, zero eigenvalues, the smallest nonzero eigenvalue, and the largest eigenvalue of (5).

In lossless cases, the eigenvalue λ_i of (5) corresponds to one resonant frequency f_i of the 3-D structure being simulated. The f_i and λ_i have the following relationship:

$$f_i = \frac{\sqrt{\lambda_i}}{2\pi}. \tag{13}$$

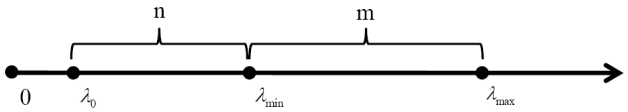

Fig. 1. Illustration of eigenvalues along the axis of λ. ($\lambda_{\min}$ is the smallest nonzero eigenvalue, $\lambda_{\max}$ is the largest eigenvalue, λ_0 is the angular frequency square corresponding to breakdown frequency).

In lossy cases, although the resonance frequency becomes complex, it has the same relationship with the eigenvalue of the numerical system.

Theoretically speaking, a 3-D structure can have an infinitely large number of resonant frequencies. In reality, the number of resonant frequencies that can be numerically found is limited because of finite mesh size. Let the smallest nonzero resonance frequency be $f_{\min}$ and the largest be $f_{\max}$, with their corresponding eigenvalues being $\lambda_{\min}$ and $\lambda_{\max}$, respectively. The $f_{\min}$ is determined by the largest physical dimension of the structure; while $f_{\max}$ that can be numerically identified is determined by the smallest mesh size. Therefore, the ratio between $f_{\max}$ and $f_{\min}$ is proportional to the ratio between the largest physical dimension of the structure and the smallest mesh size, in other words, the aspect ratio of the problem being considered. Since the eigenvalue λ_i is the square of the resonance frequency as can be seen from (13), the ratio of $\lambda_{\max}$ to $\lambda_{\min}$ is the square of the aspect ratio. We denote the distance between $\lambda_{\max}$ and $\lambda_{\min}$ in terms of orders of magnitude by m. Their relative locations are illustrated in Fig. 1 along the axis of eigenvalue λ. Besides nonzero eigenvalues from $\lambda_{\min}$ to $\lambda_{\max}$, (5) has a large nullspace, the eigenvalues of which are analytically known to be zero.

Next, we examine the relationship between the breakdown frequency, 0, $\lambda_{\min}$, and $\lambda_{\max}$. Since the root cause of low-frequency breakdown problem is finite machine precision, at the frequency where a full-wave solution breaks down, the corresponding $\omega^2\mathbf{T}$ should be beyond what can be captured by machine precision with respect to $\mathbf{S}$. In double precision computing, such an ω^2 should be 16 orders of magnitude smaller than $\|\mathbf{T}^{-1}\mathbf{S}\|$, and hence $\lambda_{\max}$. We denote such a breakdown ω^2 by $\lambda_0 = \omega^2$. Thus, if the distance between λ_0 and $\lambda_{\min}$ is n, then $n = 16 - m$, as illustrated in Fig. 1. The frequency corresponding to λ_0 is denoted by f_0, at and below of which the breakdown occurs. The n is always greater than 0 since m is less than 16. This is because as long as one can mesh the structure with a computer having finite precision, the difference between $\lambda_{\max}$ and $\lambda_{\min}$ is within machine precision.

Now it is ready to examine the existence of f_{ref}. From Fig. 1, it can be seen that f_{ref} should be above f_0 so that the full-wave solution does not break down yet and well below $f_{\min}$ so that the nonzero higher order eigenmodes can be neglected without losing accuracy. In other words, f_{ref} should fall into the range between f_0 and $f_{\min}$. Therefore, the angular frequency square corresponding to f_{ref}, $\lambda_{\text{ref}} = (2\pi f_{\text{ref}})^2$, should be between λ_0 and $\lambda_{\min}$. To ensure good accuracy, λ_{ref} should be chosen at least two orders magnitude smaller than $\lambda_{\min}$ to obtain better than 1% accuracy. As a result, for f_{ref}, and hence λ_{ref} to exist, n shown in Fig. 1 should be no less than 2.

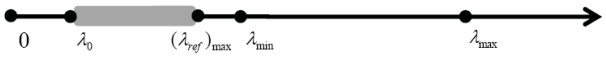

Fig. 2. Illustration of the possible range for λ_{ref}.

The condition of $n \geq 2$ is well satisfied in most problems encountered today. We can use an IC as an example to quantitatively examine n. Driven by Moore's law, the smallest feature size of ICs has been kept pushing down to the nanometer regime. Compared with the aspect ratio encountered in other engineering systems, the difference between the largest geometrical scale and the smallest scale present in today's ICs can be viewed as one of the largest. This is also the major reason why the low-frequency breakdown problem is found to be most critical in IC problems. In these problems, the ratio between the largest and the smallest feature size is approximately 1 cm versus 10 nm, which is 10^6. Thus, the ratio of $f_{\max}$ to $f_{\min}$ is 10^6, and hence the ratio of $\lambda_{\max}$ to $\lambda_{\min}$ is 10^{12}. Therefore, $m = 12$, and hence $n > 2$. As a result, as can be seen from the grey region in Fig. 2, there is a range between λ_0 and $(\lambda_{\text{ref}})_{\max}$, from which we can select any frequency to serve as f_{ref} with good accuracy achieved. Here, the $(\lambda_{\text{ref}})_{\max}$ is the largest λ_{ref} that can be chosen based on required accuracy.

It is worth mentioning that in future technologies in which the smallest feature size will be pushed further down, for example, to two orders of magnitude smaller than currently available; while the largest feature size remains similar, then $\lambda_{\max}$ will be pushed four orders of magnitude higher along the axis of λ with $\lambda_{\min}$ remained almost the same as before. In this case, $n < 2$ can happen. Then we cannot find a frequency at which the field solution is dominated by dc eigenmodes while the full-wave solution has not broken down yet. In other words, when the full-wave solution breaks down due to finite machine precision, some higher order eigenmodes will also make important contributions to the field solution. For this case, the theoretically rigorous method for handling the low-frequency problem developed in [1] and [9] is equally valid. As for the proposed fast low-frequency solution, in addition to the one vector shown in (9) that covers the contribution from all the dc eigenmodes for a given excitation, we can extend the algorithm to cover a few other vectors that characterize higher order eigenmodes. This will be considered in the future when there is a practical need for such a solution.

Next, we show how to develop a fast low-frequency full-wave solution in an $O(1)$ system for problems that involve nonideal conductors. Rigorously speaking, when low frequencies are considered, conductors cannot be treated as perfect conductors because fields penetrate into conductors at low frequencies.

IV. Proposed Fast Low-Frequency Full-Wave Solution for Problems With Nonideal Conductors

A. Theoretical Basis of the Proposed Fast Solution

Consider a problem that involves both inhomogeneous dielectric materials and nonideal conductors. We divide field

unknowns x in (1) into two groups: unknowns outside conductors x_o and unknowns inside conductors x_i. For unknowns that reside on the conducting surface, we categorize them into x_i. The FEM-based system matrix $A(\omega)$ shown in (1) can be correspondingly cast into the following form:

$$\mathbf{A}(\omega) = \begin{bmatrix} \mathbf{A}_{oo}(\omega) & \mathbf{A}_{oi}(\omega) \\ \mathbf{A}_{io}(\omega) & \mathbf{A}_{ii}(\omega) \end{bmatrix} \tag{14}$$

where

$$\begin{aligned} \mathbf{A}_{oo}(\omega) &= \mathbf{S}_{oo} - \omega^2 \mathbf{T}_{oo} \\ \mathbf{A}_{oi}(\omega) &= \mathbf{S}_{oi} - \omega^2 \mathbf{T}_{oi} \\ \mathbf{A}_{io}(\omega) &= \mathbf{S}_{io} - \omega^2 \mathbf{T}_{io} \\ \mathbf{A}_{ii}(\omega) &= \mathbf{S}_{ii} + j\omega \mathbf{R}_{ii} - \omega^2 \mathbf{T}_{ii}. \end{aligned} \tag{15}$$

In [10] and [11], a rigorous solution of $A(\omega)$'s inverse is explicitly derived, which is applicable from high frequencies down to any low frequency including dc. With a common excitation used in the FEM-based analysis, which is a current source launched outside conductors, the right-hand-side vector of (1) can be written as

$$b(\omega) = \{-j\omega I \ 0\}^T \tag{16}$$

where the first row corresponds to x_o, and the second row corresponds to x_i. At low frequencies where the contribution from higher order eigenmodes can be neglected without losing accuracy, it is shown in [10] and [11] that the field solution inside conductors (x_i) and that outside conductors (x_o) can be explicitly written as

$$\begin{aligned} x_o &= \left(-\frac{1}{\omega^2} V_0 V_0^T + \frac{1}{j\omega} \mathbf{Q} V_{ii,0} V_{ii,0}^T \mathbf{Q}^T \right) (-j\omega I) \\ x_i &= -\frac{1}{j\omega} V_{ii,0} V_{ii,0}^T \ \mathbf{Q}^T (-j\omega I) \end{aligned} \tag{17}$$

where

$$\mathbf{Q} = V_0 V_0^T \mathbf{T}_{oi} + V_h (\Lambda_h)^{-1} V_h^T \mathbf{S}_{oi} \tag{18}$$

V_0 and V_h, respectively, represent the nullspace eigenvectors and higher order eigenvectors of the system outside conductors; and $V_{ii,0}$ denotes the nullspace eigenvectors of the system inside conductors.

A careful examination of (17) reveals that the low-frequency solution can be expanded by two groups of vectors

$$\Phi_1 = \begin{pmatrix} -\mathbf{Q} V_{ii,0} \\ V_{ii,0} \end{pmatrix} \text{ and } \Phi_2 = \begin{pmatrix} V_0 \\ 0 \end{pmatrix} \tag{19}$$

which span the real and imaginary part of the solution, respectively. The number of column vectors in Φ_1 is equal to the number of dc modes of the system inside conductors; the number of column vectors in Φ_2 is equal to the number of dc modes for what's outside the conductor. The total number of vectors in $[\Phi_1, \ \Phi_2]$ is the same as that of the dc modes of the entire stiffness matrix $\mathbf{S}$, i.e., the size of the nullspace of $\mathbf{S}$. In addition, all the vectors in $[\Phi_1, \ \Phi_2]$ are linearly independent with each other, which can be easily proved because V_0 and $V_{ii,0}$ each contain linearly independent eigenvectors, and the two eigenvector sets are also mutually independent. In addition, $[\Phi_1, \ \Phi_2]$ resides in the nullspace of stiffness matrix $\mathbf{S}$. In other words, $[\Phi_1, \ \Phi_2]$ satisfies

$$S[\Phi_1, \ \Phi_2] = 0. \tag{20}$$

This can be proved as follows:

$$\begin{aligned} \mathbf{S}[\Phi_1, \ \Phi_2] &= \begin{pmatrix} \mathbf{S}_{oo} & \mathbf{S}_{oi} \\ \mathbf{S}_{io} & \mathbf{S}_{ii} \end{pmatrix} \begin{pmatrix} -\mathbf{Q} V_{ii,o} & V_0 \\ V_{ii,o} & 0 \end{pmatrix} \\ &= \begin{pmatrix} (\mathbf{S}_{oi} - \mathbf{S}_{oo}\mathbf{Q}) V_{ii,o} & \mathbf{S}_{oo} V_0 \\ (\mathbf{S}_{ii} - \mathbf{S}_{io}\mathbf{Q}) V_{ii,o} & \mathbf{S}_{io} V_0 \end{pmatrix} \end{aligned} \tag{21}$$

which is zero. To see this clearly, let us analyze the matrix entries one by one. Based on the rigorous solution developed in [10] and [11], the second-column entries in the last matrix shown in (21), $\mathbf{S}_{oo} V_0$ and $\mathbf{S}_{io} V_0$, can be immediately recognized as zero because V_0, the nullspace eigenvectors of the system outside conductors, represents a gradient-type field solution that satisfies $\nabla \times \mathbf{E} = 0$. In the first-column entries, $(\mathbf{S}_{ii} - \mathbf{S}_{io}\mathbf{Q}) V_{ii,0}$ is zero because $V_{ii,0}$ is the nullspace of $(\mathbf{S}_{ii} - \mathbf{S}_{io} Q)$ [10], [11]; $(\mathbf{S}_{oi} - \mathbf{S}_{oo}\mathbf{Q}) V_{ii,0}$ is zero because it is $(\mathbf{A}_{oi} - \mathbf{A}_{oo}\mathbf{Q}) V_{ii,o}$ at dc, and $\mathbf{Q}$, as shown in (18), is nothing but $\mathbf{A}_{oo}^{-1}\mathbf{A}_{oi}$ at dc. Hence, we prove that (21) is zero, thus $[\Phi_1, \ \Phi_2]$ belongs to the nullspace of $\mathbf{S}$. Since the dimension of $[\Phi_1, \ \Phi_2]$ is the same as the nullspace of stiffness matrix $\mathbf{S}$, and (20) holds true, we conclude that $[\Phi_1, \ \Phi_2]$ constitutes a complete nullspace of stiffness matrix $\mathbf{S}$.

Like in cases with ideal conductors, the dimension of the nullspace encountered in cases with nonideal conductors also linearly grows with matrix size $\mathbf{N}$. To shrink the dimension of the space where the field solution resides for constructing a fast low-frequency solution, a method similar to that developed for cases with ideal conductors can be developed. The details are as follows. With right-hand side $b(\omega)$ known in (16), it can be seen from (17) that the real part of the low-frequency solution x, $re(x)$, is nothing but a superposition of the vectors in Φ_1; the imaginary part of the low-frequency solution x, $im(x)$, is nothing but a superposition of the vectors in Φ_2. With $b(\omega)$, all the nullspace vectors in Φ_1 are grouped together, yielding a single vector wr-based representation of $re(x)$ as shown in the following:

$$re(x) = \begin{pmatrix} re(x_o) \\ re(x_i) \end{pmatrix} = \begin{pmatrix} -\mathbf{Q} V_{ii,0} V_{ii,0}^T \mathbf{Q}^T I \\ V_{ii,0} V_{ii,0}^T \mathbf{Q}^T I \end{pmatrix} = wr. \tag{22}$$

Similarly, all the nullspace vectors in Φ_2 are grouped together via $b(\omega)$, yielding a single vector wi-based representation of $im(x)$ as shown in the following:

$$im(x) = \begin{pmatrix} im(x_o) \\ im(x_i) \end{pmatrix} = \begin{pmatrix} \frac{1}{\omega} V_0 V_0^T I \\ 0 \end{pmatrix} = wi. \tag{23}$$

The two vectors wr and wi form a complete space for representing the field solution of (2) at low frequencies. This finding again holds true for problems with inhomogeneous lossless and/or lossy dielectrics as well as problems filled with a dispersive material.

B. Proposed Fast Low-Frequency Full-Wave FEM Solution

To obtain the reduced space of $O(1)$ composed of wr and wi and also avoid solving the eigenvalue problem, similar to

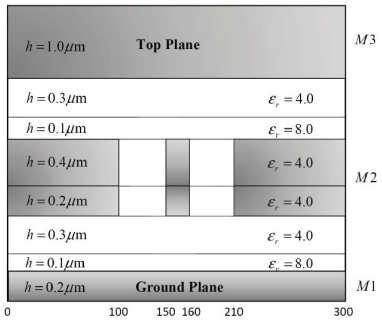

Fig. 3. Illustration of an on-chip 3-D interconnect.

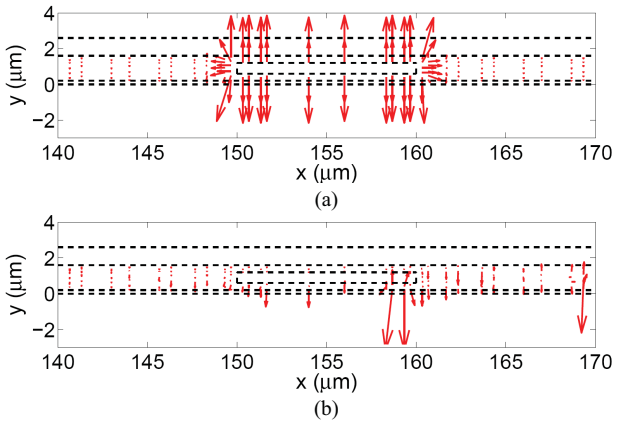

Fig. 4. **E** field distribution of a 3-D on-chip interconnect at 10^{-32} Hz. (a) Proposed method. (b) Conventional full-wave FEM method.

the approach developed for cases with ideal conductors, at one frequency f_{ref} whose corresponding angular frequency square is between λ_0 and $(\lambda_{\text{ref}})_{\max}$, we solve the original system (1) to obtain the field solution x_{ref}. Different from cases with ideal conductors, we separate this solution into two vectors, namely, the real part x_{re} and the imaginary part x_{im}. The x_{re} constitutes the same $O(1)$ space as that formed by wr, while x_{im} represents the same $O(1)$ space formed by wi. Next, we use x_{re} and x_{im} to form space

$$z = [x_{re}, x_{im}]. \tag{24}$$

Expanding field solution in this space, and testing the system by the same space, we obtain a reduced system of order one as follows:

$$z^T(\mathbf{S} - \omega^2\mathbf{T} + j\omega\mathbf{R})z\ y = z^T b(\omega). \tag{25}$$

Again, this reduced system still experiences the low-frequency breakdown problem because of finite machine precision. To overcome this problem, we vanish $z^T\mathbf{S}z$ based on the fact shown in (20). Thus, we have

$$z^T(-\omega^2\mathbf{T} + j\omega\mathbf{R})z\ y = z^T b(\omega). \tag{26}$$

The left-hand-side matrix of (26) is a 2×2 matrix. Apparently, the solution of (26) can still break down at low frequencies since **T**- and **R**-related terms have different frequency dependence. However, this problem does not exist in (26) because (26) is a diagonal matrix (the proof is given in the Appendix) as shown in the following:

$$\begin{pmatrix} -\omega^2\widetilde{\mathbf{T}} & 0 \\ 0 & j\omega\widetilde{\mathbf{R}} \end{pmatrix} y = z^T b(\omega) \tag{27}$$

where

$$\begin{aligned} \widetilde{\mathbf{R}} &= x_{re}^T\mathbf{R}x_{re} = x_{re,i}^T\mathbf{R}_{ii}x_{re,i} \\ \widetilde{\mathbf{T}} &= x_{im}^T\mathbf{T}x_{im} = x_{im,o}^T\mathbf{T}_{oo}x_{im,o}. \end{aligned} \tag{28}$$

After the diagonal 2×2 system shown in (27) is solved, y is known. The solution of the original system (1) can then be readily obtained from

$$x(\omega) = zy. \tag{29}$$

By doing so, we obtain the field solution at any low frequency including dc. As can be seen from the above procedure, instead of introducing additional computational cost into a full-wave solver, the proposed method accelerates the full-wave computation at low frequencies.

V. Numerical Results

In order to validate the proposed method, we simulated a number of on-chip and package examples.

The first example is a 3-D on-chip interconnect embedded in inhomogeneous materials shown in Fig. 3. In this figure, the detailed geometrical and material parameters are given. The structure is of length 2000 μm. Along the length direction, the front and the back end each is attached to an air layer, which is then truncated by a Neumann-type boundary condition. The top and bottom planes shown in Fig. 3 are backed by a perfect electric conducting (PEC) boundary condition. The left and right boundary conditions are Neumann-type boundary conditions. The shaded region is occupied by conductors. To validate the proposed fast solution for cases with ideal conductors, the conductor is assumed to be perfect. The cases with conductor loss will be considered in the third example. A current source of 1 A is launched from the bottom plane to the center conductor in the $M2$ layer. The smallest mesh size is 0.1 μm. For this example, a traditional full-wave solver breaks down at $\sim$10 MHz. In our simulation, we choose $f_{\text{ref}} = 100$ MHz (the reason is given later in this section) and solve the original system (1) at this frequency to obtain x_{ref}. The field solution at any lower frequency including dc is then solved from (10) and (12). In Fig. 4(a), we plot the electric field distribution at 10^{-32} Hz in the transverse plane of the 3-D interconnect simulated by the proposed method. In Fig. 4(b), we plot the electric field distribution simulated by a conventional full-wave FEM solver. Clearly, the proposed method produces an accurate electric field distribution, whereas the traditional solver breaks down. In Table I, we compare the results generated by the proposed solution and those obtained from the rigorous solution developed in [1] and [9] that solved a generalized eigenvalue problem shown in (5). The capacitances extracted by these two solutions agree very well with each other. The relative error of the proposed solution is shown to be very small compared to the rigorous solution. It is clear that the proposed fast low-

TABLE I
COMPARISON OF THE CAPACITANCES OF A 3-D INTERCONNECT STRUCTURE

Frequency (Hz)	Capacitance (F)		Solution relative error
	The rigorous solution [1], [9]	The proposed fast solution	
1e8	4.4852e-12	4.4853e-12	8.9415e-04
1e5	4.4851e-12	4.4853e-12	8.9169e-04
1e3	4.4851e-12	4.4853e-12	8.9169e-04
1e-1	4.4851e-12	4.4853e-12	8.9169e-04
1e-16	4.4851e-12	4.4853e-12	8.9169e-04
1e-32	4.4851e-12	4.4853e-12	8.9169e-04

frequency solution preserves the accuracy of the theoretically rigorous solution in [1] and [9] while eliminating the need for solving an eigenvalue problem.

Since the proposed solution utilizes the solution vector obtained at one frequency, f_{ref}, to obtain the field solution at any low frequency where a traditional full-wave solver would break down, one might be interested to know how the f_{ref} is determined in this example. The f_{ref} is analytically estimated from the geometrical and mesh data based on the theoretical analysis given in Section III-C. First, we analytically estimate $f_{\min}$, $f_{\max}$, and f_0, which are found to be $f_{\min} \sim 3 \times 10^{10}$ Hz, $f_{\max} \sim 6.7 \times 10^{14}$ Hz, and $f_0 \sim 1 \times 10^7$ Hz. In our estimation, a uniform material with an effective permittivity is used. These estimation results agree very well with numerical data, in which $f_{\min}$ and $f_{\max}$ are shown to be 3.8×10^{10} and 1×10^{15} Hz, respectively. As mentioned, the conventional full-wave solver breaks down at $\sim$10 MHz. This agrees with our analytical prediction since the square of this breakdown frequency is 16 orders of magnitude smaller than $\lambda_{\max}$. From the estimated $f_{\min}$ and f_0, we know that f_{ref} can be arbitrarily chosen between 1×10^7 and 3×10^9 Hz with good accuracy. This range is above f_0 and one order of magnitude smaller than $f_{\min}$ so that the resultant λ_{ref} is at least two orders of magnitude smaller than $\lambda_{\min}$. This is how $f_{\text{ref}} = 100$ MHz is determined.

Next, in order to demonstrate the capability of the proposed solver in solving problems with a dispersive material, we consider a parallel plate structure filled with a material with complicated frequency dependence. The width, height, and length of the structure are set to be 10, 1, and, 35 μm, respectively, in accordance with the typical dimensions of on-chip circuits. The dielectric material between two PEC plates is FR4, which is modeled by the following dielectric loss model [15]:

$$\varepsilon_r(\omega) = \varepsilon'_\infty + \frac{\Delta\varepsilon'}{1 + j\frac{\omega}{\omega_0}} \tag{30}$$

where $\varepsilon'_\infty = 4.9$, $\Delta\varepsilon' = 0.28$, and $\omega_0 = 2 \times 10^6 \text{s}^{-1}$. A current source of 1 A is injected from the bottom plane to the top plane. The smallest edge length used in discretization is 1 μm. We analytically estimate $f_0 \sim 1 \times 10^6$, $f_{\min} \sim 1.9 \times 10^{12}$, and $f_{\max} \sim 6.7 \times 10^{13}$ Hz. These data are in good agreement with the actual data, which are shown to be

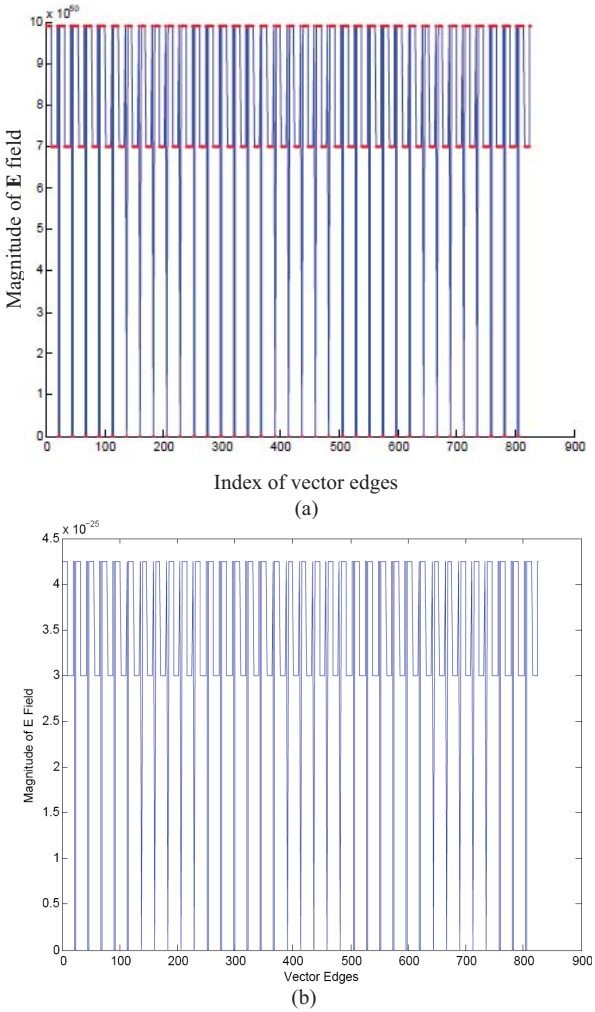

Fig. 5. Electric field simulated at each edge at 10^{-32} Hz. (a) Proposed method (in red dots) and rigorous method [10], [11] (in blue line). (b) Conventional full-wave FEM method.

1.9×10^{12} Hz for $f_{\min}$ and 1×10^{14} Hz for $f_{\max}$. In addition, we examine the 1-norm of $\omega^2\mathbf{T}$ over that of $\mathbf{S}$, we find that it is larger than machine precision when frequency is higher than 6×10^6 Hz, which agrees with the fact that the conventional full-wave FEM solver breaks down at $\sim$1 MHz. Based on these analytical estimations, we choose 100 MHz as f_{ref} in this simulation. In Fig. 5(a), we plot the electric field at each edge in the computational domain at 10^{-32} Hz simulated by the proposed method in comparison with that obtained from the rigorous method developed in [10] and [11]. Two results agree very well with each other and both exhibit an open circuit phenomenon. In contrast, the traditional full-wave FEM solver gives very small field values, which is wrong, as shown in Fig. 5(b). In Table II, we compare the admittances simulated using the proposed method, the rigorous solution [10], [11], and a conventional FEM solver. It is clear that the proposed solution agrees very well with the rigorous solution, whereas the conventional FEM solver is totally wrong at low frequencies.

The last example involves both inhomogeneous dielectrics and nonideal conductors. It is a 3-D loop inductor residing

TABLE II
ADMITTANCE EXTRACTED BY THREE METHODS

Frequency (Hz)	Real part of the admittance (1/Ω)			Imaginary part of the admittance (1/Ω)		
	Proposed solution	Rigorous solution [10], [11]	Conventional full-wave method	Proposed solution	Rigorous solution [10], [11]	Conventional full-wave method
10^{8}	2.7581597e-18	2.75815973e-18	2.758159737e-18	1.5163937646e-14	1.516393756e-14	1.516349335e-14
10^{7}	2.75539591e-17	2.7553958e-17	2.755395883e-17	1.5164805934e-14	1.5164805852e-14	1.51510056e-14
10^{6}	2.50443535e-16	2.50443533e-16	2.477684473e-16	1.5243647519e-14	1.5243647435e-14	1.18176313e-14
10^{5}	2.47768450e-16	2.477684473e-16	2.504435330e-16	1.595260031e-14	1.5952600245e-14	−3.7530252e-13
10^{3}	2.72219529e-18	2.72219526e-18	2.722195262e-18	1.6030430535e-14	1.6030430446e-14	−3.7530252e-09
10^{-1}	2.72222216e-22	2.72222212e-22	0	1.603043909e-14	1.6030438998e-14	−0.3753025
10^{-16}	2.72222216e-37	2.72222216e-37	2.72222212e-37	1.603043909e-14	1.6030438998e-14	−3.7530252e+29
10^{-32}	2.72222216e-53	2.72222212e-53	2.722222129e-53	1.603043909e-14	1.6030438998e-14	−3.7530252e+61

TABLE III
INPUT IMPEDANCE COMPARISON

Frequency (Hz)	Real Part of the Input Impedance (Ω)			Imaginary Part of the Input Impedance (Ω)		
	Proposed Solution	Rigorous Solution [10], [11]	Conventional Full-wave Method	Proposed Solution	Rigorous Solution [10], [11]	Conventional Full-Wave Method
10^{7}	2.7484e-1	2.7413e-1	2.7413e-1	−1.6252e4	−1.6252e4	−1.6252e4
10^{5}	2.7484e-1	2.7300e-1	2.4058e-1	−1.6252e6	−1.6252e6	−1.6412e6
10^{3}	2.7484e-1	2.7300e-1	1.9373e8	−1.6252e8	−1.6252e8	3.2457e8
10^{-1}	2.7484e-1	2.7300e-1	−23.6	−1.6252e12	−1.6252e12	349.0
10^{-16}	2.7484e-1	2.7300e-1	−6.051e-10	−1.6252e27	−1.6252e27	−2.638e-11
10^{-32}	2.7484e-1	2.7300e-1	−5.000e-40	−1.6252e43	−1.6252e43	−7.8598e-22
0	2.7484e-1	2.7300e-1	0	∞	∞	0

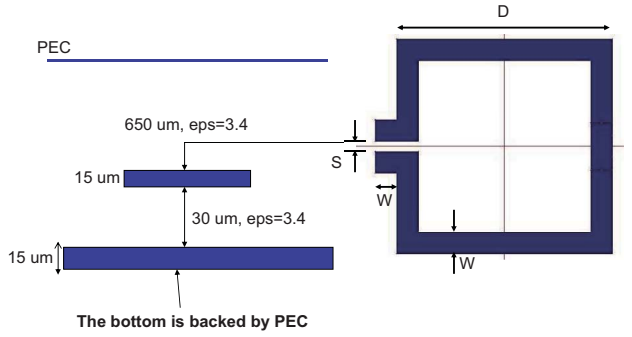

Fig. 6. Geometry and material of a 3-D loop inductor.

on a package. The geometry of the loop inductor is shown in Fig. 6. Its diameter (D) is 1000 μm. The metallic wire is 100-μm wide and 15-μm thick. The metal conductivity is 5.8×10^{7}. The port separation (S) is 50 μm. The inductor is backed by two package planes. The backplane is 15-μm thick. In this simulation, the smallest mesh size is 10 μm in dielectric regions. Based on an analytical estimation, $f_{\min}$ and $f_{\max}$ are found to be ∼15 and ∼1.5×10^{4} GHz, respectively. Moreover, we can estimate that f_0 is between 0.1 and 1 MHz, which is also verified by the simulation based on the conventional full-wave solver. Based on $f_{\min}$ and f_0, we chose 10 MHz as f_{ref} in this simulation. In Table III, we compare the input impedance simulated by three solutions at low frequencies: the proposed solution, the rigorous solution [10], [11], and the conventional full-wave FEM solution. It is clear that among the three solutions, the proposed solution is in an excellent agreement with the rigorous solution, both of which can generate correct frequency dependence for real and imaginary parts. It is worth mentioning that the input impedance is extracted between one port of the inductor and the bottom reference ground with the other port left open. In Table III, at zero frequency, the imaginary part of the input impedance is infinity, which is analytically obtained from the proposed method as can be seen from the first row of (17). Moreover, in order to verify our theoretical analysis of $[\Phi_1,\ \Phi_2]$, we checked the number of dc modes for the system inside and outside the conductor. One is 356 and the other is 365. Their addition is 721, which is exactly the number of dc modes of the entire $\mathbf{S}$ matrix.

VI. CONCLUSION

It has been observed that a full-wave solution of Maxwell's equations breaks down at low frequencies. In order to efficiently eliminate the low-frequency breakdown problem, this paper presents a fast low-frequency full-wave finite-element-based solution, for both problems involving ideal conductors and problems with nonideal conductors immersed in inhomogeneous, lossless, lossy, and dispersive materials. It retains the theoretical rigor of the solution developed in [1] and [9]–[11], while eliminating the need for an eigenvalue solution. We have identified that the low-frequency solution is dominated by the nullspace of the stiffness matrix. Although the dimension of the nullspace grows linearly with the problem size, we show that a single solution vector obtained at one low frequency serves as a complete space for representing the contribution from all the nullspace vectors for a given excitation. Therefore, utilizing one such vector, we reduce the original system of $O(N)$ to an $O(1)$ system. By dropping the resultant stiffness matrix rigorously based on the fact that the field solution is in the nullspace of the

stiffness matrix, we successfully bypass the barrier of finite machine precision that is the root cause of low-frequency breakdown and, also, solve the breakdown problem efficiently. Instead of introducing additional computational cost to fix the low-frequency breakdown problem, the proposed method significantly speeds up the low-frequency computation. When simulating a frequency band from high to low frequencies, the cost of the proposed method is $O(1)$ at all the breakdown frequencies since the single solution vector used to obtain the solution at low frequencies is available for use. When simulating only low frequencies where a full-wave solver breaks down, the proposed method will first generate a solution at a reference frequency and then use this solution to obtain the solution at the desired frequencies. In this case, the proposed method does not introduce additional computational cost to fix the low-frequency breakdown problem either. In addition, the proposed method can be used to capture complicated frequency dependence at low frequencies due to material dispersion and conductor loss.

Moreover, the reduced space of $O(1)$ identified in this paper serves as a complete representation of the contribution from all the nullspace vectors, i.e., dc eigenmodes, for a given excitation. Such an $O(1)$ space not only can be used to rapidly fix the low-frequency breakdown problem in FEMs, but also can be employed by other frequency- and time-domain methods for fast and accurate low-frequency analysis. In addition, the proposed $O(1)$ space effectively shrinks the dimension of the original nullspace that grows linearly with the problem size, and hence can be used in other applications where nullspace vectors are required.

We have also theoretically analyzed the relationship between zero frequency, breakdown frequency, the first nonzero eigenvalue, and the highest eigenvalue of the numerical system; from which we demonstrated the validity of the proposed $O(1)$ solution in technologies that are available today. For future technologies or applications in which not only dc eigenmodes but also higher order eigenmodes contribute to the solution at the breakdown frequency, the proposed $O(1)$ space can be flexibly expanded to cover a few other vectors that characterize nonzero higher order modes in addition to the single vector that represents the contribution from all dc modes, with the total cost still minimized to be negligible.

A large part of this paper is devoted to derivations that serve as the theoretical basis of the proposed fast solution. For a quick reference, readers can refer to Sections III-B and IV-B, which is the outcome of the proposed research. As can be seen from these two sections, the implementation of the proposed fast low-frequency full-wave solution is user friendly.

APPENDIX

Here, we prove that (27) is a diagonal matrix.

Based on (22), the x_{re} in (24) can be compactly written as

$$x_{re} = \begin{pmatrix} -\mathbf{Q}V_{ii,0}y_i \\ V_{ii,0}y_i \end{pmatrix} \tag{A.1}$$

where $y_i = V_{ii,0}^T \mathbf{Q}^T I$ denotes the coefficient vector that carries the weight of each nullspace eigenvector in field solution. Similarly, based on (23), the x_{im} in (24) can be compactly written as

$$x_{im} = \begin{pmatrix} V_0 y_o \\ 0 \end{pmatrix} \tag{A.2}$$

where $y_o = V_0^T I/\omega$. By using (A.1) and (A.2), we have

$$z^T(-\omega^2\mathbf{T} + j\omega\mathbf{R})z = \begin{pmatrix} -y_i^T(\mathbf{Q}V_{ii,0})^T & y_i^T(V_{ii,0})^T \\ y_0^T V_0^T & 0 \end{pmatrix} \times \begin{pmatrix} -\omega^2\mathbf{T}_{oo} & -\omega^2\mathbf{T}_{oi} \\ -\omega^2\mathbf{T}_{io} & j\omega\mathbf{R}_{ii} \end{pmatrix} \begin{pmatrix} -\mathbf{Q}V_{ii,0}y_i & V_0 y_o \\ V_{ii,0}y_i & 0 \end{pmatrix}. \tag{A.3}$$

By utilizing the following fact:

$$\mathbf{T}_{oo}\mathbf{Q}V_{ii,0}y_i - \mathbf{T}_{oi}V_{ii,0}y_i = 0 \tag{A.4}$$

it can be readily derived that the off-diagonal terms of (A.3) are zero. Next, we show why (A.4) holds true.

Since x_{re} and x_{im} are obtained from a field solution x_{ref} that satisfies (1), from (14) and (16), the x_{ref}s components x_o and x_i satisfy

$$\mathbf{A}_{oo}(\omega)x_o + \mathbf{A}_{oi}(\omega)x_i = -j\omega I. \tag{A.5}$$

Thus

$$\mathbf{A}_{oo}(\omega)x_{re,o} + \mathbf{A}_{oi}(\omega)x_{re,i} = 0 \tag{A.6}$$

where $x_{re,o}$ is the real part of x_o, and $x_{re,i}$ is the real part of x_i. Since $x_{re,o} = -\mathbf{Q}V_{ii,0}y_i$ and $x_{re,i} = V_{ii,0}y_i$, as can be seen from (A.1), we have

$$(\mathbf{S}_{oo} - \omega^2\mathbf{T}_{oo})(-\mathbf{Q}V_{ii,0}y_i) + (\mathbf{S}_{oi} - \omega^2\mathbf{T}_{oi})(V_{ii,0}y_i) = 0 \tag{A.7}$$

which can be further written as

$$(S_{oi} - S_{oo}\mathbf{Q})V_{ii,0}y_i + \omega^2(\mathbf{T}_{oo}\mathbf{Q}V_{ii,0}y_i - \mathbf{T}_{oi}V_{ii,0}y_i) = 0. \tag{A.8}$$

Since $(S_{oi} - S_{oo}\mathbf{Q})V_{ii,0} = 0$ as shown in Section IV.A, (A.4) is obtained.

In addition to recognizing that (A.3) is diagonal, the derivation of (27) also utilizes the fact that the displacement current can be neglected inside conductors compared to conduction current from dc to very high frequencies.

REFERENCES

[1] J. Zhu and D. Jiao, "A theoretically rigorous full-wave finite-element-based solution of Maxwell's equations from dc to high frequencies," *IEEE Trans. Adv. Packag.*, vol. 33, no. 4, pp. 1043–1050, Nov. 2010.

[2] J. Zhao and W. C. Chew, "Integral equation solution of Maxwell's equations from zero frequency to microwave frequencies," *IEEE Trans. Antennas Propag.*, vol. 48, no. 10, pp. 1635–1645, Oct. 2000.

[3] S. Lee and J. Jin, "Application of the tree-cotree splitting for improving matrix conditioning in the full-wave finite-element analysis of high-speed circuits," *Microw. Opt. Technol. Lett.*, vol. 50, no. 6, pp. 1476–1481, Jun. 2008.

[4] R. Wang, D. J. Riley, and J. Jin, "Application of tree-cotree splitting to the time-domain finite-element analysis of electromagnetic problems," *IEEE Trans. Antennas Propag.*, vol. 58, no. 5, pp. 1590–1600, May 2010.

[5] Z. G. Qian and W. Chew, "Fast full-wave surface integral equation solver for multiscale structure modeling," *IEEE Trans. Antennas Propag.*, vol. 57, no. 11, pp. 3594–3602, Nov. 2009.

[6] Z. G. Qian and W. Chew, "Enhanced A-EFIE with pertubation method," *IEEE Trans. Antennas Propag.*, vol. 58, no. 10, pp. 3256–3264, Oct. 2004.

[7] R. J. Adams, "Physical properties of a stabilized electric field integral equation," *IEEE Trans. Antennas Propag.*, vol. 52, no. 10, pp. 3256–3264, Oct. 2010.

[8] S. Yan, J. Jin, and Z. Nie, "EFIE analysis of low-frequency problems with loop-star decomposition and Calderon multiplicative preconditioner," *IEEE Trans. Antennas Propag.*, vol. 58, no. 3, pp. 857–867, Mar. 2010.

[9] J. Zhu and D. Jiao, "A theoretically rigorous solution for fundamentally eliminating the low-frequency breakdown problem in finite-element-based full-wave analysis," in *Proc. IEEE Int. Symp. Antennas Propag.*, Jul. 2010, pp. 1–4.

[10] J. Zhu and D. Jiao, "A rigorous method for fundamentally eliminating the low-frequency break-down in full-wave finite-element-based analysis: Combined dielectric-conductor case," in *Proc. IEEE 19th Conf. Electr. Perform. Electron. Packag. Syst.*, Oct. 2010, pp. 1–4.

[11] J. Zhu and D. Jiao, "A rigorous solution to the low-frequency breakdown in full-wave finite-element-based analysis of general problems involving inhomogeneous lossless/lossy dielectrics and non-ideal conductors," *IEEE Trans. Microw. Theory Tech.*, vol. 59, no. 12, pp. 3294–3306, Dec. 2011.

[12] J. Lee, V. Balakrishnan, C.-K. Koh, and D. Jiao, "From O(k^2N) to O(N): A fast complex-valued eigenvalue solver for large-scale on-chip interconnect analysis," *IEEE Trans. Microw. Theory Tech.*, vol. 57, no. 12, pp. 3219–3228, Dec. 2009.

[13] J. Lee, D. Chen, V. Balakrishnan, C.-K. Koh, and D. Jiao, "A quadratic eigenvalue solver of linear complexity for 3-D electromagnetics-based analysis of large-scale integrated circuits," *IEEE Trans. Comput.-Aided Design*, vol. 31, no. 3, pp. 380–390, Mar. 2012.

[14] J. Zhu, S. Omar, W. Chai, and D. Jiao, "A rigorous solution to the low-frequency breakdown in the electric field integral equation," in *Proc. IEEE Int. Symp. Antennas Propag.*, Jul. 2011, pp. 1–4.

[15] A. R. Djordjevic, R. M. Biljic, V. D. Likar-Smiljanic, and T. K. Sarkar, "Wideband frequency-domain characterization of FR-4 and time-domain causality," *IEEE Trans. Electromagn. Compat.*, vol. 43, no. 4, pp. 662–667, Nov. 2001.

Jianfang Zhu received the B.S. degree in electronic engineering and information science from the University of Science and Technology of China, Hefei, China, in 2006, and the Ph.D. degree in electrical engineering from Purdue University, West Lafayette, IN, in August 2011.

She is currently a Senior Engineer with the Hard IP Group, Intel Corporation, Santa Clara, CA. Her current research interests include computational and applied electromagnetics, high-frequency VLSI design and analysis, multiscale multiphysics modeling, signal integrity, and power integrity analysis.

Dr. Zhu was a finalist of the Best Student Paper Award from the IEEE International Symposium on Antennas and Propagation in 2010. One of her papers was also among the three finalists for the IEEE Transactions on Advanced Packaging Best Paper Award in 2010. Her dissertation was nominated for the Dimitris N. Chorafas Foundation Award for an Outstanding Ph.D. Thesis. She won the Best Undergraduate Thesis Award and the Outstanding Student Scholarship from the University of Science and Technology of China.

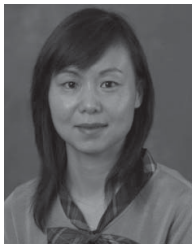

Dan Jiao (S'00–M'02–SM'06) received the Ph.D. degree in electrical engineering from the University of Illinois at Urbana-Champaign, Urbana, in 2001.

She was with the Technology Computer-Aided Design (CAD) Division, Intel Corporation, until September 2005, as a Senior CAD Engineer, Staff Engineer, and a Senior Staff Engineer. She joined Purdue University, West Lafayette, IN, in September 2005, as an Assistant Professor with the School of Electrical and Computer Engineering, where she is currently a tenured Associate Professor. She has authored two book chapters and over 160 papers in refereed journals and international conference proceedings. Her current research interests include computational electromagnetics, high-frequency digital, analog, mixed-signal, and RF integrated circuit (IC) design and analysis, high-performance VLSI CAD, modeling of microscale and nanoscale circuits, applied electromagnetics, fast and high-capacity numerical methods, fast time-domain analysis, scattering and antenna analysis, RF, microwave, and millimeter-wave circuits, wireless communication, and bio-electromagnetics.

Dr. Jiao has served as a reviewer for many IEEE journals and conferences. She is an Associate Editor of the IEEE TRANSACTIONS ON COMPONENTS, PACKAGING, AND MANUFACTURING TECHNOLOGY. She was among the 100 engineers selected throughout the nation for the National Academy of Engineering's U.S. Frontiers of Engineering Symposium in 2011. She was the recipient of the Ruth and Joel Spira Outstanding Teaching Award in 2010, the National Science Foundation CAREER Award in 2008, the Jack and Cathie Kozik Faculty Start-up Award (which recognizes an outstanding new faculty member of the School of Electrical and Computer Engineering, Purdue University) in 2006, the Office of Naval Research Award under the Young Investigator Program in 2006, the Best Paper Award from the Intel Corporation's annual corporate-wide technology conference (Design and Test Technology Conference) for her work on generic broadband model of high-speed circuits in 2004, the Intel Corporation's Logic Technology Development (LTD) Divisional Achievement Award in recognition of her work on the industry-leading BroadSpice modeling/simulation capability for designing high-speed microprocessors, packages, and circuit boards, in 2003, the Intel Corporation's Technology CAD Divisional Achievement Award for the development of innovative full-wave solvers for high-frequency IC design, the Intel Corporation's Components Research the Intel Hero Award (she was the tenth recipient Intel-wide) for the timely and accurate 2-D and 3-D full-wave simulations in 2002, the Intel Corporation's LTD Team Quality Award for her outstanding contribution to the development of the measurement capability and simulation tools for high-frequency on-chip crosstalk, and the Raj Mittra Outstanding Research Award presented by the University of Illinois at Urbana-Champaign in 2000.